Letter

Optically induced spin current in monolayer $NbSe_2$

Ren Habara [1] and Katsunori Wakabayashi [1,2,3]

[1] *Department of Nanotechnology for Sustainable Energy, School of Science and Technology, Kwansei Gakuin University, Gakuen 2-1, Sanda 669-1337, Japan*

[2] *National Institute for Materials Science (NIMS), Namiki 1-1, Tsukuba 305-0044, Japan*

[3] *Center for Spintronics Research Network (CSRN), Osaka University, Toyonaka 560-8531, Japan*

(Received 23 March 2021; revised 17 April 2021; accepted 20 April 2021; published 27 April 2021)

Monolayer $NbSe_2$ is a metallic two-dimensional (2D) transition-metal dichalcogenide material. Owing to the lattice structure and the strong atomic spin-orbit coupling (SOC) field, monolayer $NbSe_2$ possesses Ising-type SOC which acts as an effective Zeeman field, leading to the unconventional topological spin properties. In this paper, we numerically calculate spin-dependent optical conductivity of monolayer $NbSe_2$ using Kubo formula based on an effective tight-binding model which includes d_{z^2}, $d_{x^2-y^2}$, and d_{xy} orbitals of Nb atoms. Numerical calculation indicates that the up- and down-spin have opposite sign of Hall current, so the pure spin Hall current can be generated in monolayer $NbSe_2$ under light irradiation, owing to the topological nature of monolayer $NbSe_2$, i.e., finite spin Berry curvature. The spin Hall angle is also evaluated. The optically induced spin Hall current can be enhanced by the electron doping and persists even at room temperature. Our results will serve to design opt-spintronics devices such as *spin current harvesting by light irradiation* on the basis of 2D materials.

DOI: 10.1103/PhysRevB.103.L161410

Transition-metal dichalcogenide (TMDC) is a class of two-dimensional (2D) electronic systems and provides a platform to design functional opt-electronic devices [1–5]. In TMDCs, electronic properties crucially depend on the combination of metal and chalcogen atoms [6,7]. Because of weak van der Waals forces between layers, monolayers of TMDCs can be easily exfoliated and exhibit many fascinating properties such as valley-dependent optical selection rule [8–11] and spin Hall effect (SHE) [12–15]. In particular, monolayer $NbSe_2$ belongs to monolayer of group-V TMDC MX_2 ($M =$ Nb, Ta; $X =$ S, Se), and is known to show metallic behavior with a superconducting phase transition at low temperatures [16–19]. Monolayer $NbSe_2$ has a hexagonal lattice structure but with no spatial inversion symmetry and possesses out-of-plane mirror symmetry. Owing to the lattice structure and a strong atomic spin-orbit coupling (SOC) field, monolayer $NbSe_2$ possesses Ising-type SOC, [17–23], i.e., an effective Zeeman field that locks electron spin to out-of-plane directions by in-plane momentum and provides unconventional topological spin properties.

In this paper, we show that pure spin Hall current can be generated in monolayer $NbSe_2$ by light irradiation, owing to the topological nature of monolayer $NbSe_2$, i.e., finite spin Berry curvature. Figures 1(a) and 1(b) show the top and side views of monolayer $NbSe_2$, respectively, where a layer of Nb atoms is sandwiched by two layers of Se atoms. From the top view, monolayer $NbSe_2$ has a hexagonal lattice structure but with no spatial inversion symmetry. Also, from the side view, it respects out-of-plane mirror symmetry. Figure 1(c) shows the corresponding first Brillouin zone (BZ). We employ a multiorbital tight-binding model (TBM) which includes d_{z^2}, $d_{x^2-y^2}$, and d_{xy} orbitals of Nb atoms to describe the electronic states of $NbSe_2$ [17,24]. The eigenvalue equation for TBM is $\hat{H}(\boldsymbol{k})|u_{n\boldsymbol{k}}\rangle = E_{n\boldsymbol{k}}|u_{n\boldsymbol{k}}\rangle$, where $\boldsymbol{k} = (k_x, k_y)$ is the wave-number vector, $E_{n\boldsymbol{k}}$ is the eigenvalue and $n = 1, 2, \cdots, 6$ is the band index. The eigenvector is defined as $|u_{n\boldsymbol{k}}\rangle = (c_{n\boldsymbol{k},d_{z^2},\uparrow}, c_{n\boldsymbol{k},d_{xy},\uparrow}, c_{n\boldsymbol{k},d_{x^2-y^2},\uparrow}, c_{n\boldsymbol{k},d_{z^2},\downarrow}, c_{n\boldsymbol{k},d_{xy},\downarrow}, c_{n\boldsymbol{k},d_{x^2-y^2},\downarrow})^T$, where $(\cdots)^T$ indicates the transpose of the vector and $c_{n\boldsymbol{k}\tau s}$ means the amplitude at atomic orbital τ with spin s for the nth energy band at $\boldsymbol{k}$. The Hamiltonian with the SOC can be written as

$$\hat{H}(\boldsymbol{k}) = \hat{\sigma}_0 \otimes \hat{H}_{\rm TNN}(\boldsymbol{k}) + \hat{\sigma}_z \otimes \tfrac{1}{2}\lambda_{\rm SOC}\hat{L}_z, \tag{1}$$

with

$$\hat{H}_{\rm TNN}(\boldsymbol{k}) = \begin{pmatrix} V_0 & V_1 & V_2 \\ V_1^* & V_{11} & V_{12} \\ V_2^* & V_{12}^* & V_{22} \end{pmatrix} \tag{2}$$

and

$$\hat{L}_z = \begin{pmatrix} 0 & 0 & 0 \\ 0 & 0 & -2i \\ 0 & 2i & 0 \end{pmatrix}. \tag{3}$$

Here, $\hat{\sigma}_0$ and $\hat{\sigma}_z$ are Pauli matrices and $\lambda_{\rm SOC}$ is the Ising-type SOC parameter. In monolayer $NbSe_2$, $\lambda_{\rm SOC} = 0.0784$ eV. $\hat{H}_{\rm TNN}(\boldsymbol{k})$ includes the electron hoppings only among three d orbitals of Nb atoms, which are assumed up to third-nearest neighbor (NN) sites as shown in Fig. 1(a). Here, green, red, and blue arrows indicate hopping vectors $\boldsymbol{R_i}$ $(i = 1, 2, \cdots, 6)$ pointing to NN sites, the vectors $\tilde{\boldsymbol{R}}_{\boldsymbol{j}} (j = 1, 2, \cdots, 6)$ pointing to next-NN sites, and the vectors $2\boldsymbol{R_i}$ pointing to third-NN sites, respectively. The details of matrix elements V_0, V_1, V_2, V_{11}, V_{12}, and V_{22} can be found in Supplemental Material [25]. Figure 1(d) shows the energy band structure of monolayer

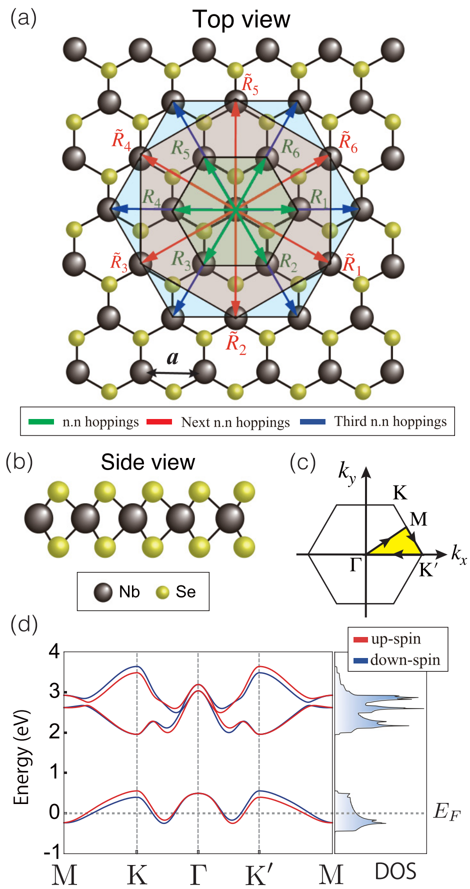

FIG. 1. Crystal structure of monolayer $NbSe_2$ which consists of Nb (black) and Se (yellow) atoms. (a) Top view and (b) side view of the lattice structure. Green, red, and blue arrows indicate hopping vectors $\boldsymbol{R}_i$ $(i = 1, 2, \cdots, 6)$ pointing to NN sites, the vectors $\tilde{\boldsymbol{R}}_j$ $(j = 1, 2, \cdots, 6)$ pointing to next-NN sites, and the vectors $2\boldsymbol{R}_i$ pointing to third-NN sites, respectively. a is the lattice constant. (c) First BZ of monolayer $NbSe_2$. (d) Energy band structure and DOS of $NbSe_2$ with SOC parameter $\lambda_{\rm SOC} = 0.0784$ eV. Fermi level is set to zero.

$NbSe_2$ along the line passing through the high-symmetric points of the first BZ and the corresponding density of states (DOS). Here, red and blue lines indicate spin-up and spin-down states. Monolayer $NbSe_2$ is metallic, but with a large energy band gap between the partially filled valence bands and empty conduction bands. Also, the Ising-type SOC provides the opposite spin splitting at the valence band edges in K and K′ points, and time-reversal symmetry protection.

We numerically calculate spin-dependent optical conductivity of $NbSe_2$ using Kubo formula [26–35] based on an effective TBM and find the photoinduced generation of pure spin Hall current [36–38]. The spin-dependent optical Hall conductivity can be given as

$$\sigma_{xy}^{\rm spin}(\omega) = \frac{i\hbar e}{S}\sum_{\boldsymbol{k}}\sum_{nm}\frac{f(E_{n\boldsymbol{k}}) - f(E_{m\boldsymbol{k}})}{E_{m\boldsymbol{k}} - E_{n\boldsymbol{k}}} \times \frac{\langle u_{n\boldsymbol{k}}|\hat{j}_x^{\rm spin}|u_{m\boldsymbol{k}}\rangle\,\langle u_{m\boldsymbol{k}}|\hat{v}_y|u_{n\boldsymbol{k}}\rangle}{E_{m\boldsymbol{k}} - E_{n\boldsymbol{k}} - \hbar\omega - i\eta}, \tag{4}$$

where $n(m)$ indicates the band index including spin degree of freedom, $|u_{n\boldsymbol{k}}\rangle$ is the eigenfunction with the eigenenergy $E_{n\boldsymbol{k}}$ and $f(E_{n\boldsymbol{k}})$ is Fermi-Dirac distribution function. η is an infinitesimally small real number and S is the area of system. Also, $\hat{j}_x^{\rm spin}$ is the spin current operator and written as $\hat{j}_x^{\rm spin} = \frac{1}{2}\{\frac{\hbar}{2}\hat{\sigma}_z \otimes \hat{I}_3, \hat{v}_x\}$, where $\hat{I}_3$ is the 3×3 identity matrix and $(\hat{v}_x, \hat{v}_y) = \frac{1}{\hbar}(\frac{\partial \hat{H}}{\partial x}, \frac{\partial \hat{H}}{\partial y})$ is the group velocity operator. We add the superscript *spin* for the spin-dependent optical Hall conductivity to distinguish its conductivity from ordinary optical Hall conductivity without SOC. When we consider $\sigma_{xy}^{\rm spin}(\omega)$ for direct current (DC) limit ($\omega = 0$), zero-temperature ($T = 0$ K), and clean limit ($\eta = 0$ eV), Eq. (14) becomes

$$\sigma_{xy}^{\rm spin} = \frac{e}{S}\sum_{\boldsymbol{k}}\Omega^{\rm spin}(\boldsymbol{k}) \tag{5}$$

with

$$\Omega^{\rm spin}(\boldsymbol{k}) = \hbar\sum_{n} f(E_{n\boldsymbol{k}})\sum_{m\neq n}\frac{-2{\rm Im}\,\langle u_{n\boldsymbol{k}}|\hat{j}_x^{\rm spin}|u_{m\boldsymbol{k}}\rangle\,\langle u_{m\boldsymbol{k}}|\hat{v}_y|u_{n\boldsymbol{k}}\rangle}{(E_{m\boldsymbol{k}} - E_{n\boldsymbol{k}})^2}. \tag{6}$$

Here, $\Omega^{\rm spin}(\boldsymbol{k})$ is spin Berry curvature of Bloch state, [26,33,39–46] and drives an anomalous transverse velocity

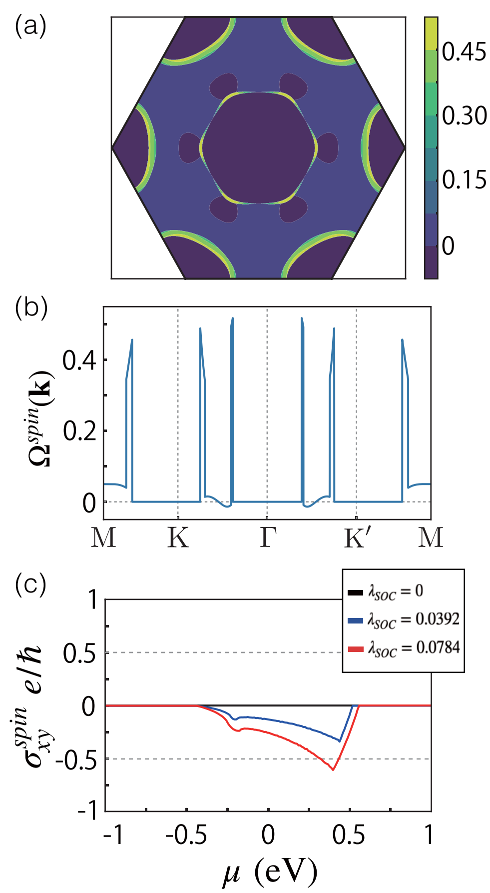

FIG. 2. Spin Berry curvature of monolayer $NbSe_2$ with SOC parameter $\lambda_{\rm SOC} = 0.0784$ eV. (a) Contour plot in first BZ. (b) Plot along the path through the high-symmetric points in 1st BZ. (c) Fermi-level dependence of spin-dependent Hall conductivity $\sigma_{xy}^{\rm spin}$ of DC limit for several different SOC parameters. The unit of $\sigma_{xy}^{\rm spin}$ is $e^2/\hbar$.

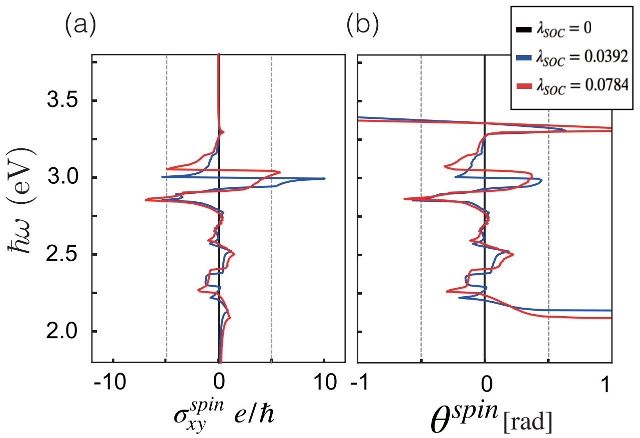

FIG. 3. Optical angular frequency dependence of (a) spin-dependent Hall conductivity $\sigma_{xy}^{\rm spin}(\omega)$ of $E_F = 0$ eV and (b) SHA $\theta^{\rm spin}$ for several different SOC parameters. The unit of $\sigma_{xy}^{\rm spin}(\omega)$ is $e^2/\hbar$.

[47,48] written as

$$v_\perp = -\frac{e}{\hbar}\boldsymbol{E} \times \Omega^{\rm spin}(\boldsymbol{k}) \tag{7}$$

under the presence of an electric field $\boldsymbol{E}$.

Figure 2(a) shows the 2D contour plot of spin Berry curvature in the first BZ. It clearly shows the sixfold symmetry. However, for each spin state, its symmetry around the Γ point reduces to threefold symmetry because the energy band of monolayer $NbSe_2$ has opposite spin splitting around K and K′ points [see Figs. S2(a) and S2(b)] [25]. In Fig. 2(b), the spin Berry curvature is plotted along the path passing through high-symmetric points of the first BZ. Owing to the Fermi-Dirac distribution function in Eq. (6), the spin Berry curvature is vanished at the valleys. This is in contrast to a semiconducting MX_2 such as MoS_2, where valley current is induced owing to the finite Berry curvature at the valleys. In monolayer $NbSe_2$, valley current can be induced by the electron doping [see Figs. S4(a) and S4(b)] [25]. As can be seen in Fig. 2(b), the spin Berry curvature has sharp peaks with the same sign, because the energy differences between up- and down-spin states become very small at the Fermi energy, as can be confirmed in Fig. 1(d). Figure 2(c) shows Fermi energy dependence of spin-dependent Hall conductivity for several different SOC parameters. Since spin Hall conductivity is the summation of the spin Berry curvature over the momentum in the DC limit, it can be calculated by using Eq. (5). It is noted that the spin Hall conductivity is enhanced by electron doping. Thus, finite Berry curvature manifests the intrinsic SHE [45–47], i.e., the generation of transverse spin current by the application of electric field.

Figure 3(a) shows the numerically calculated angular frequency dependence of spin-dependent optical Hall conductivity for several different SOC parameters. It is clearly seen that the large peak around 3.0 eV, i.e., the generation of spin Hall current in $NbSe_2$ ($\lambda_{\rm SOC} = 0.0784$ eV) by light irradiation. The cases for $\lambda_{\rm SOC} = 0.0392$ and 0 eV are also plotted for comparison. It should be noted that the optical charge Hall conductivity is identically zero for arbitrary energy because the charge Berry curvature has antisymmetry with the wave number, i.e., $\Omega^{\rm charge}(\boldsymbol{k}) = -\Omega^{\rm charge}(-\boldsymbol{k})$ [see Figs. S2(c) and S2(d)] [25]. Thus, the pure spin current can be induced by light irradiation in monolayer $NbSe_2$. Since the intensive peaks of $\sigma_{xy}^{\rm spin}$ appear in the range of 2.7 − 3.2 eV, i.e., visible and ultraviolet range, monolayer $NbSe_2$ can be used for the application of *spin current harvesting by light irradiation*. The effect of optically induced spin Hall current is also robust to temperature, and is expected to be observed even at room temperature [see Fig. S5 (a)] [25].

Figure 3(b) shows the angular frequency dependence of the spin Hall angle (SHA) [26,36,46,49,50], which measures conversion efficiency from charge current to spin current. SHA is given as

$$\theta^{\rm spin} = \frac{2e}{\hbar}\frac{\sigma_{xy}^{\rm spin}}{\sigma_{xx}}, \tag{8}$$

where σ_{xx} is optical longitudinal conductivity [31,51,52] which is found in Fig. S5(b) [25]. SHA has divergence below about 2.1 eV and above about 3.3 eV, because σ_{xx} becomes zero, where SHA becomes ill-defined. When the Hall conductivity has a peak, the SHA also has larger value and then indicates that we can generate the pure spin current efficiently. Moreover, the observed optically induced pure Hall spin current is robust against the carrier doping. In particular, the pure spin current can be enhanced by electron doping (see Fig. S6) [25]. These results indicate that we can generate the spin Hall current efficiently by light irradiation using the visible light of violet and enhance its magnitude by electron doping.

In conclusion, we have theoretically proposed that pure spin Hall current can be induced efficiently in monolayer $NbSe_2$ by irradiating the visible light. The origin of spin Hall current can be attributed to the finite spin Berry curvature owing to the Ising-type SOC in monolayer $NbSe_2$. It is also found that the optically induced spin Hall current can be enhanced by the electron doping and persists even at room temperature (see Supplemental Material) [25]. Thus, monolayer $NbSe_2$ can be used for the source of pure spin current by using light irradiation. Our results will serve to design opt-spintronics devices such as *spin current harvesting by light irradiation* on the basis of 2D materials.

This work was supported by JSPS KAKENHI (Grants No. JP21H01019 and No. JP18H01154) and JST CREST (Grant No. JPMJCR19T1).

[1] K. F. Mak, C. Lee, J. Hone, J. Shan, and T. F. Heinz, Phys. Rev. Lett. **105**, 136805 (2010).
[2] A. Splendiani, L. Sun, Y. Zhang, T. Li, J. Kim, C.-Y. Chim, G. Galli, and F. Wang, Nano Lett. **10**, 1271 (2010).
[3] S. Tongay, J. Zhou, C. Ataca, K. Lo, T. S. Matthews, J. Li, J. C. Grossman, and J. Wu, Nano Lett. **12**, 5576 (2012).
[4] H. R. Gutiérrez, N. Perea-López, A. L. Elías, A. Berkdemir, B. Wang, R. Lv, F. López-Urías, V. H.

Crespi, H. Terrones, and M. Terrones, Nano Lett. **13**, 3447 (2013).
[5] W. Zhao, Z. Ghorannevis, L. Chu, M. Toh, C. Kloc, P.-H. Tan, and G. Eda, ACS Nano **7**, 791 (2013).
[6] Q. H. Wang, K. Kalantar-Zadeh, A. Kis, J. N. Coleman, and M. S. Strano, Nat. Nanotechnol. **7**, 699 (2012).
[7] M. Chhowalla, H. S. Shin, G. Eda, L.-J. Li, K. P. Loh, and H. Zhang, Nat. Chem. **5**, 263 (2013).
[8] H. Zeng, J. Dai, W. Yao, D. Xiao, and X. Cui, Nat. Nanotechnol. **7**, 490 (2012).
[9] K. F. Mak, K. He, J. Shan, and T. F. Heinz, Nat. Nanotechnol. **7**, 494 (2012).
[10] T. Cao, G. Wang, W. Han, H. Ye, C. Zhu, J. Shi, Q. Niu, P. Tan, E. Wang, B. Liu, and J. Feng, Nat. Commun. **3**, 887 (2012).
[11] H. Yu, X. Cui, X. Xu, and W. Yao, Natl. Sci. Rev. **2**, 57 (2015).
[12] J. Sinova, S. O. Valenzuela, J. Wunderlich, C. H. Back, and T. Jungwirth, Rev. Mod. Phys. **87**, 1213 (2015).
[13] P. N. Hai, J. Magn. Soc. Jpn. **44**, 137 (2020).
[14] Y. K. Kato, R. C. Myers, A. C. Gossard, and D. D. Awschalom, Science **306**, 1910 (2004).
[15] J. Wunderlich, B. Kaestner, J. Sinova, and T. Jungwirth, Phys. Rev. Lett. **94**, 047204 (2005).
[16] S. Kim and Y.-W. Son, Phys. Rev. B **96**, 155439 (2017).
[17] W.-Y. He, B. T. Zhou, J. J. He, N. F. Q. Yuan, T. Zhang, and K. T. Law, Commun. Phys. **1**, 40 (2018).
[18] X. Xi, Z. Wang, W. Zhao, J.-H. Park, K. T. Law, H. Berger, L. Forró, J. Shan, and K. F. Mak, Nat. Phys. **12**, 139 (2016).
[19] E. Sohn, X. Xi, W.-Y. He, S. Jiang, Z. Wang, K. Kang, J.-H. Park, H. Berger, L. Forró, K. T. Law, J. Shan, and K. F. Mak, Nat. Mater. **17**, 504 (2018).
[20] J. M. Lu, O. Zheliuk, I. Leermakers, N. F. Q. Yuan, U. Zeitler, K. T. Law, and J. T. Ye, Science **350**, 1353 (2015).
[21] Y. Saito, Y. Nakamura, M. S. Bahramy, Y. Kohama, J. Ye, Y. Kasahara, Y. Nakagawa, M. Onga, M. Tokunaga, T. Nojima, Y. Yanase, and Y. Iwasa, Nat. Phys. **12**, 144 (2016).
[22] B. T. Zhou, N. F. Q. Yuan, H.-L. Jiang, and K. T. Law, Phys. Rev. B **93**, 180501(R) (2016).
[23] L. Bawden, S. P. Cooil, F. Mazzola, J. M. Riley, L. J. Collins-McIntyre, V. Sunko, K. W. B. Hunvik, M. Leandersson, C. M. Polley, T. Balasubramanian, T. K. Kim, M. Hoesch, J. W. Wells, G. Balakrishnan, M. S. Bahramy, and P. D. C. King, Nat. Commun. **7**, 11711 (2016).
[24] G.-B. Liu, W.-Y. Shan, Y. Yao, W. Yao, and D. Xiao, Phys. Rev. B **88**, 085433 (2013).
[25] See Supplemental Material at http://link.aps.org/supplemental/10.1103/PhysRevB.103.L161410 for details of matrix elements in an effective Hamiltonian. The doping and temperature effects on optical spin Hall conductivity are also presented.
[26] J. Qiao, J. Zhou, Z. Yuan, and W. Zhao, Phys. Rev. B **98**, 214402 (2018).
[27] G. Y. Guo, Y. Yao, and Q. Niu, Phys. Rev. Lett. **94**, 226601 (2005).
[28] P. Sengupta and E. Bellotti, J. Appl. Phys. **120**, 123105 (2016).
[29] V. Vargiamidis, P. Vasilopoulos, and G.-Q. Hai, J. Phys. Condens. Matter **26**, 345303 (2014).
[30] T. Tanaka, H. Kontani, M. Naito, T. Naito, D. S. Hirashima, K. Yamada, and J. Inoue, Phys. Rev. B **77**, 165117 (2008).
[31] A. Ferreira, J. Viana-Gomes, Y. V. Bludov, V. Pereira, N. M. R. Peres, and A. H. Castro Neto, Phys. Rev. B **84**, 235410 (2011).
[32] T. Morimoto, Y. Hatsugai, and H. Aoki, Phys. Rev. Lett. **103**, 116803 (2009).
[33] Y. Yao, L. Kleinman, A. H. MacDonald, J. Sinova, T. Jungwirth, D.-s. Wang, E. Wang, and Q. Niu, Phys. Rev. Lett. **92**, 037204 (2004).
[34] Z. Li and J. P. Carbotte, Phys. Rev. B **86**, 205425 (2012).
[35] M. Akita, Y. Fujii, M. Maruyama, S. Okada, and K. Wakabayashi, Phys. Rev. B **101**, 085418 (2020).
[36] S. Y. Huang, D. Qu, T. C. Chuang, C. C. Chiang, W. Lin, and C. L. Chien, Appl. Phys. Lett. **117**, 190501 (2020).
[37] W. Lin and C. L. Chien, arXiv:1804.01392.
[38] W.-Y. Shan, J. Zhou, and D. Xiao, Phys. Rev. B **91**, 035402 (2015).
[39] J. Sławińska, F. T. Cerasoli, H. Wang, S. Postorino, A. Supka, S. Curtarolo, M. Fornari, and M. B. Nardelli, 2D Mater. **6**, 025012 (2019).
[40] Y. Yao and Z. Fang, Phys. Rev. Lett. **95**, 156601 (2005).
[41] H. Da, Q. Song, P. Dong, H. Ye, and X. Yan, J. Appl. Phys. **127**, 023903 (2020).
[42] M. Gradhand, D. V. Fedorov, F. Pientka, P. Zahn, I. Mertig, and B. L. Györffy, J. Phys. Condens. Matter **24**, 213202 (2012).
[43] G. Qu, K. Nakamura, and M. Hayashi, arXiv:1901.05651.
[44] J. Kim, K.-W. Kim, D. Shin, S.-H. Lee, J. Sinova, N. Park, and H. Jin, Nat. Commun. **10**, 3965 (2019).
[45] G. Y. Guo, S. Murakami, T.-W. Chen, and N. Nagaosa, Phys. Rev. Lett. **100**, 096401 (2008).
[46] J. Zhou, J. Qiao, A. Bournel, and W. Zhao, Phys. Rev. B **99**, 060408(R) (2019).
[47] W. Feng, Y. Yao, W. Zhu, J. Zhou, W. Yao, and D. Xiao, Phys. Rev. B **86**, 165108 (2012).
[48] D. Xiao, M.-C. Chang, and Q. Niu, Rev. Mod. Phys. **82**, 1959 (2010).
[49] Y. Wang, P. Deorani, X. Qiu, J. H. Kwon, and H. Yang, Appl. Phys. Lett. **105**, 152412 (2014).
[50] W. Zhang, W. Han, S.-H. Yang, Y. Sun, Y. Zhang, B. Yan, and S. S. P. Parkin, Sci. Adv. **2**, e1600759 (2016).
[51] R. Kubo, J. Phys. Soc. Japan **12**, 570 (1957).
[52] S. Saberi-Pouya, T. Vazifehshenas, T. Salavati-fard, M. Farmanbar, and F. M. Peeters, Phys. Rev. B **96**, 075411 (2017).